

## Improved Localization of Implanted Subdural Electrode Contacts on MRI Using an Elastic Image Fusion Algorithm in Invasive EEG Recording

Lennart Henning Stieglitz, MD<sup>1</sup>, Christian Ayer, MD<sup>2</sup>, Kaspar Schindler, MD<sup>3</sup>, Markus Florian Oertel, MD<sup>4</sup>, Roland Wiest, MD<sup>5</sup>, Claudio Pollo, MD<sup>4</sup>

<sup>1</sup>Department of Neurosurgery, Zurich University Hospital, University of Zurich, Zurich, Switzerland

<sup>2</sup>University of Bern, Bern, Switzerland

<sup>3</sup>Department of Neurology, <sup>4</sup>Department of Neurosurgery, <sup>5</sup>Diagnostic and Interventional Neuroradiology, Inselspital, Bern University Hospital and University of Bern, Bern, Switzerland

### Corresponding Author:

Lennart Henning Stieglitz, MD

Department of Neurosurgery

Zurich University Hospital

8091 Zurich, Switzerland

e-mail: [lennart.stieglitz@usz.ch](mailto:lennart.stieglitz@usz.ch)

Tel: +41 44 255 31 22/Fax: +41 44 255 57 41

**Disclosure:** The authors have no competing interests. No specific funding was provided for this project. The providers of the software tested had no role in study design, data collection, data analysis, decision to publish, or preparation of the manuscript.

## **Abstract**

**Background:** Accurate projection of implanted subdural electrode contacts in presurgical evaluation of pharmacoresistant epilepsy cases by invasive EEG is highly relevant. Linear fusion of CT and MRI images may display the contacts in the wrong position due to brain shift effects.

**Objective:** A retrospective study in five patients with pharmacoresistant epilepsy was performed to evaluate whether an elastic image fusion algorithm can provide a more accurate projection of the electrode contacts on the pre-implantation MRI as compared to linear fusion.

**Methods:** An automated elastic image fusion algorithm (AEF), a guided elastic image fusion algorithm (GEF), and a standard linear fusion algorithm (LF) were used on preoperative MRI and post-implantation CT scans. Vertical correction of virtual contact positions, total virtual contact shift, corrections of midline shift and brain shifts due to pneumocephalus were measured.

**Results:** Both AEF and GEF worked well with all 5 cases. An average midline shift of 1.7mm (SD 1.25) was corrected to 0.4mm (SD 0.8) after AEF and to 0.0mm (SD 0) after GEF. Median virtual distances between contacts and cortical surface were corrected by a significant amount, from 2.3mm after LF to 0.0mm after AEF and GEF ( $p < .001$ ). Mean total relative corrections of 3.1 mm (SD 1.85) after AEF and 3.0mm (SD 1.77) after GEF were achieved. The tested version of GEF did not achieve a satisfying virtual correction of pneumocephalus.

**Conclusion:** The technique provided a clear improvement in fusion of pre- and post-implantation scans, although the accuracy is difficult to evaluate.

**Running Title:** Elastic Fusion in Invasive Recording

**Keywords:** EEG, elastic image fusion, epilepsy, invasive recording

## INTRODUCTION

In pharmacoresistant epilepsy cases, the decision to perform invasive investigation using intracranial electroencephalography (EEG) electrodes in order to localize the epileptogenic locus is often one of the last diagnostic options. In such cases, patients and physicians are driven by the hope of identifying a region of the brain whose resection might lead to significantly improved seizure control or even complete seizure freedom and increased quality of life. There are currently several accepted surgical methods to place electrode contacts on the brain surface to identify such regions.

The first method involves performing an extensive craniotomy and positioning a multi-contact grid on the cortex.<sup>1</sup> The second but less invasive method involves stereotactic implantation of multiple electrodes inside the brain through a series of trepanations, called stereo-EEG.<sup>2,3</sup> The third and least invasive method is the implantation of 4 to 10 contact strip-electrodes on the cortex through a small number (at least one per side) of limited trepanations.<sup>4</sup> After electrode implantation, the direct positioning of the contacts on the cortex allows EEG recording with excellent signal-to-noise ratios and minimal muscle artifacts over several days, and leads to a much better delineation of the epileptogenic zone as compared to extracranially recorded EEG.<sup>5</sup> These EEG data can then be used for planning a potentially curative resective surgery, with the aim to achieve freedom from seizures.

All techniques enable exact localization of the contact position on the cortex, which is crucial for interpretation of the EEG signals. However, an imaging technology that allows visualization of metal electrode contacts and brain tissue simultaneously would be preferable. Unfortunately, MRI can cause tissue damage due to energy transfer into heat.<sup>5</sup> Furthermore, the contacts cause artifacts in most imaging sequences that are far more intensive than the signal of the contacts themselves. On the other hand, in a CT scan the contacts can be visualized easily and even without image distortion, but due to artifacts around the contacts and inferior quality of soft-tissue contrast, localization of the contacts in relation to the brain surface is also difficult.<sup>6</sup> Combination of both techniques using image fusion of preoperatively acquired MRI with

postoperative CT scans is common and provides the required spatial information, but is susceptible to the effects of brain shift. Cerebrospinal fluid (CSF) loss during electrode implantation and air trapped subdurally may cause a considerable dislocation of cortical structures.<sup>7,8</sup> A linear image fusion, allowing only translations, rotations, scaling and skewness to align two image datasets, might localize the contacts in the wrong position.<sup>9,10</sup> Elastic image fusion algorithms are a relatively new development and are not yet standard in commercial software used in neurosurgery. In addition to linear translations they allow local modifications of the image datasets to achieve a better alignment. They may be helpful for solving this problem as they theoretically can compensate for these brain shift effects and enable visualization of the actual contact positions on the gyri. To analyze the preliminary results of such an innovative approach, a retrospective study in five patients with pharmaco-resistant epilepsy was performed to evaluate whether an elastic image fusion algorithm can provide a more accurate projection of the electrode contacts on the pre-implantation MRI than simple elastic fusion.

## **METHODS**

### **Patients**

Twenty-three patients (6 males, 17 females) suffering from pharmaco-resistant epilepsy underwent an invasive recording phase between January and December 2011 at the Bern University Hospital (Inselspital). All patients had previously undergone a non-invasive recording phase, but the epileptogenic brain areas could not be as precisely localized as required to directly proceed to resective surgery.

Application of the elastic image fusion required a complete imaging dataset, which is described in detail below. A subgroup of five patients, two males and three females, with an average age of 19 years (SD 2.9), ultimately fulfilled these requirements.

### **Pre- and postoperative neuroimaging**

For the stereotactic implantation of additional hippocampal depth electrodes<sup>11</sup> all patients received pre- and postoperative CT scans. Preoperatively, the patients underwent a T2 MRI scan (T2 weighted spin echo sequence: TR=2200 ms, S=1 mm (gap 0), FOV=256 mm, matrix=256×256 on a 3 T Magnetom Verio MR system, Siemens Healthcare, Erlangen, Germany) and a

native CT scan (tube current = 180 mA, kvp = 120 kV, standard kernel, slice thickness 1 mm (supratentorial/infratentorial), and FOV = 220 mm on a GE Lightspeed 8-row detector scanner, GE Healthcare, Milwaukee, Wisconsin, USA). Postoperatively (day of surgery) all patients received an additional native CT scan as described above.

### **Electrode implantation technique**

To reduce morbidity and to allow maximal coverage of the brain surface we implanted multiple 4 to 6-contact strip electrodes in a star-like manner from frontal and frontotemporal regions via 14-mm-trepanations. To minimize the risk of infection the patient's head was shaved and iv antibiotics were given perioperatively. The ideal positions of the trepanations were localized using a neuronavigation system (VectorVision2, BrainLab, Feldkirchen, Germany). Under general anesthesia, trepanation was performed and the dura was opened. Four to eight contact strip electrodes (Ad-Tech medical instrument corporation, Racine, USA) were implanted under neuronavigation and fluoroscopic guidance (Table 1). Depending on the clinical presentation of the patient, one burr hole was placed uni- or bilaterally over the Sylvian fissure with 3 to 4 strips going around the temporal lobe and 2 to 4 strips covering the frontal and frontoparietal lobes. To reduce CSF loss, the trepanation was sealed using fibrin glue after implantation of the final electrode. The cables were subcutaneously tunneled and externalized through the skin at least 4 cm distant from the trepanation site to reduce infection. Postoperatively, the position of the electrode contacts and absence of potential subdural hematomas were confirmed on a native CT scan.

### **Image co-registration**

The most common method used for co-registration of two image datasets is the so-called mutual information (MI) method. It originates from the information theory and measures the statistical dependency between two datasets and was shown to perform well in co-registration of CT and MRI.<sup>12,13</sup> In linear co-registration the alignment of the two datasets is achieved by translation, rotation, scaling and skewness, each along three degrees of freedom (DOF), adding up to 12 DOF altogether. Elastic co-registration should be able to, in addition to the linear translation, apply changes only locally and thus deliver more precise results, especially when the image acquisition time is different or even when pre- and postoperative datasets are to be fused.

### *Linear image fusion*

All image fusions were performed using a pre-release version provided by Brainlab iPlan (Brainlab, Feldkirchen, Germany). The algorithm for linear image fusion (LF) applies 12 DOF and is identical with that included in the commercial software version iPlan 3.0. The region of interest is automatically defined and covers the entire skull of the patient. In all fusion procedures the postoperative CT scan was fused onto the preoperative MRI scan.

### *Elastic image fusion*

The elastic image fusion was performed using two different versions of the elastic fusion algorithm. The first one, referred to as automated elastic fusion (AEF), tries to find a corresponding position in the first dataset for each structure in the second. The algorithm runs fully automated.

The second one, referred to as guided elastic fusion (GEF), allows manual definition of corresponding structures in both images; during the automated fusion process, these manually-defined structures may have no counterpart in the other dataset. Examples for such structures would be tumors in pre- and postoperative images or intracranial air, which are not present in preoperative images. In the present study we segmented intracranial air for GEF.

Both algorithms allow deformation of an underlying grid in three dimensions to achieve an optimal fit of the anatomical structures. Figure 1 shows a deformation map indicating direction and intensity of deformation for each position of the grid. Just like in the linear fusion processes, the postoperative CT scans were elastically fused onto the preoperative MRI.

### **Assessment of the effect of elastic image fusion on virtual brain shift**

CSF loss and resulting pneumocephalus often lead to a lateral shift of the midline to the contralateral side. Therefore, as the most straightforward parameter, the lateralization of the midline at the level of the foramen of Monroe was measured in millimeters both after linear and after elastic image fusion using the two different software versions, AEF and GEF.

Second, the size of frontally trapped subdural air was judged in the postoperative CT after linear and after elastic image fusion. The maximum thickness in an axial slice and the volume of trapped air were measured.

After linear image fusion the electrode contacts on CT are sometimes virtually projected inside the cortex or even subcortically. An optimal fusion should enable visualization of the electrode contacts correctly on the cortical surface and should compensate for brain shift effects. To examine the ability of both elastic fusion algorithms (AEF and GEF) to achieve this, we measured the distances of the virtual contacts' positions and the brain surface, and compared the results with the position of the contacts after linear image fusion. The distances are given in millimeters and measured separately in the frontal, parietal and temporal regions. Furthermore, the shortest distance between electrode contacts after linear and elastic image fusion were measured to judge the dimension of the elastic fusion's effect.

### **Statistics and ethics**

All patient data were anonymized before import into the iPlan software. The local ethics committee approved this retrospective analysis. Statistical analyses included Welch two-sample t-test and Wilcoxon non-parametric test using "R" statistics programming language.<sup>14</sup> A p-value of less than .05 was considered significant. All values were not normally distributed (Shapiro-Wilk Normality test).

## **RESULTS**

### **Midline shift correction**

Correction of the midline shift was one of the major parameters used to evaluate elastic fusion's accuracy. As a point of reference, to measure this shift we defined an axial slice through the septum pellucidum directly above the foramen of Monro. While the median midline shift in the postoperative CT (evaluated by LF) was 1.9 mm, it was corrected to a median of 0 mm by both AEF and GEF. Due to the small number of patients included in the study, the result was not statistically significant (Table 2).

### **Pneumencephalus correction**

The second task for elastic fusion algorithms was the correction of pneumocephalus in the fused images. Neither AEF nor GEF corrected sufficiently for this problem, as shown for measurements of frontal air thickness (Table 3) and air volumetry (Table 4). Therefore, the elastic fusion algorithms used in the present study ultimately provided no significant reduction of pneumocephalus.

### **Electrode contact position**

Both AEF and GEF achieved an effective reduction of the electrode – cortex distance, as shown in Figure 2. This result was achieved in all tested areas: frontal, temporal and parietal regions. The reduction of distance compared to the linear fusion was statistically significant (Wilcoxon;  $p < .001$ ; Table 5).

### **Relative virtual electrode contact position correction**

Elastic image fusion led to relevant virtual shifts of the electrode contact positions by median distances of 2.9 mm (AEF) and 2.8 mm (GEF), respectively (Table 5). Differences between the two fusion algorithms tested in this study were not statistically significant. However, statistically significant regional differences were found for the frontal versus temporal cortices ( $p = .031$ ) and the frontal versus parietal cortices ( $p < .001$ ).

## **DISCUSSION**

Invasive recording workup for patients suffering from pharmaco-resistant epilepsy is often a stressful and demanding procedure for both the patient and the attending physician. Though the procedure can be considered safe, effective and a gold-standard, implantation of electrodes into the skull and brain exclusively for diagnostic purposes is an option that only patients desperate for treatment of their seizures will undergo. This makes it especially important that everything is done to make the results optimally useful for treatment planning. Accurate projection of the implanted electrode contacts on the brain surface is a crucial step, especially when it involves resection planning in or close to eloquent cortex. With grid implantation through craniotomy, the brain surface can be photographed and images can be superimposed onto a cortical MRI reconstruction.<sup>15-20</sup> Combinations of photography and 2-D radiography have been described,<sup>10</sup> as



have linear superpositions using a 3-D visualization system.<sup>9</sup> Contacts under the margins of the craniotomy or placed through burr-holes cannot be documented photographically; these contacts are also subject to brain shift, which can be corrected mathematically.<sup>7,20</sup>

Using the anatomical information of the CT scan and combining this with the high spatial and contact soft-tissue resolution of MRI provides a potential new option to handle this situation. Modern computers allowing highly complex calculations, together with newly developed elastic fusion algorithms, can be used to compensate for brain shift effects in the future. The algorithms tested and presented here performed the fusion in 5 to 10 minutes per case on a BrainLab iPlan server (HP ProLiant DL360p Gen 8: 2xIntel Xeon E5-2667, 2.9 GHz, 32GB RAM, 4x300 GB HDD). One possible use is the fusion of postoperative CT after subdural electrode implantation with preoperative MRI for contact superposition.

### **Display of electrode contacts on the brain surface**

Linear fusion of pre- and postoperative images often localizes the position of the electrode contacts incorrectly, often inside the cortex or even subcortically (Figures 3A and 3C). Automated elastic image fusion (AEF) led to a display of the contacts that was clearly distant from where they were shown after linear fusion. The effect was stronger in the temporal than in the frontal region, and also affected contacts implanted parietally. Some of the subgroups of contacts in different brain regions are very small and allow only limited interpretation.

After elastic fusion (both AEF and GEF) the contacts displayed were clearly closer to the brain surface (Figures 3B and 3D). However, a clear superiority of the GEF over the AEF could not be shown.

### **Plausibility of the results**

Because there are usually few landmarks visible on both CT and MRI to evaluate the quality of the elastic fusion, correction of major shift effects was used to validate the fusion results. The interhemispheric midline should normally be located in the middle of the skull. However, shifts to either side can occur after trepanation of the skull, loss of CSF, intracranial trapping of air, brain swelling, or resection of space-occupying lesions or epileptogenic brain tissue. Both elastic fusion algorithms completely compensated for the midline shift.

Originally our purpose was to develop a simple automated fusion algorithm. Unfortunately, the elastic fusion algorithms were not accurate enough to compensate for the shift caused by pneumocephalus. The finding that this algorithm did not sufficiently deal with additional volumes or non-existing volumes in either of the fused images led to the idea of creating an additional guided algorithm. The GEF has the advantage that it utilizes corresponding points or structures in both image sets to support the automated structure detection. Furthermore, a function was added to define a volume in one of the image sets that might undergo major change or might not be present in the other image set. Potential examples therefore might be a tumor removed, a hematoma evacuated, or intracranial air inoculated.

Validation of elastic image fusion results is very difficult in cases where there is no way to document the electrode contact positions visually. A photographic documentation of the electrode contact positions would have been preferable -- as shown by Tao et al,<sup>17</sup> LaViolette et al,<sup>18</sup> and Pieters et al,<sup>19</sup> in cases where a grid was implanted through a craniotomy. Dykstra et al,<sup>20</sup> faced the same problem as we do with localizing electrode contacts that are implanted through burr-holes. Not being able to compare with intraoperative photographs, they simply shift the electrode contacts to the level of the pia.

## **CONCLUSION**

We demonstrated that elastic fusion can produce more plausible results than the linear fusion, but the available algorithms must be developed further to deal with complex situations, such as fusing pre- and postoperative images.

The technique is fast, fully automated, and offers high flexibility. The scope of possible applications of the presented software is not limited to epilepsy surgery. Another possible field of application would be fusion of pre- and postoperative images after tumor resection to better identify the position of tumor remnants in the preoperative MRI.

## **Further software development**

We thank BrainLab, Germany for kindly providing the two elastic fusion algorithms used in this study. The software applied in the present study was constantly refined. The results presented here do not necessarily represent the abilities of the most recent software version, as experiences and results driven from our work directly influenced the further development of the software.

## REFERENCES

1. Vadera S, Mullin J, Bulacio J, Najm I, Bingaman W, Gonzalez-Martinez J. Stereoelectroencephalography following subdural grid placement for difficult to localize epilepsy. *Neurosurgery*. 2013;72(5):723-9; discussion 729. doi:10.1227/NEU.0b013e318285b4ae.
2. Gonzalez-Martinez J, Mullin J, Vadera S, et al. Stereotactic placement of depth electrodes in medically intractable epilepsy. *J Neurosurg*. 2014. doi:10.3171/2013.11.JNS13635.
3. Bancaud J, Talairach J. *La Stéréo-ÉlectroEncéphaloGraphie dans l'épilepsie*. Paris: Masson & Cie; 1965:35-122.
4. Wyler AR, Ojemann GA, Lettich E, Ward AA. Subdural strip electrodes for localizing epileptogenic foci. *J Neurosurg*. 1984;60(6):1195-200. doi:10.3171/jns.1984.60.6.1195.
5. Bhavaraju NC, Nagaraddi V, Chetlapalli SR, Osorio I. Electrical and thermal behavior of non-ferrous noble metal electrodes exposed to MRI fields. *Magn Reson Imaging*. 2002;20(4):351-7. Available at: <http://www.ncbi.nlm.nih.gov/pubmed/12165354>. Accessed August 12, 2013.
6. Hastreiter P, Rezk-Salama C, Soza G, et al. Strategies for brain shift evaluation. *Med Image Anal*. 2004;8(4):447-64. doi:10.1016/j.media.2004.02.001.
7. Hermes D, Miller KJ, Noordmans HJ, Vansteensel MJ, Ramsey NF. Automated electrocorticographic electrode localization on individually rendered brain surfaces. *J Neurosci Methods*. 2010;185(2):293-8. doi:10.1016/j.jneumeth.2009.10.005.
8. Serra C, Huppertz H-J, Kockro RA, et al. Rapid and accurate anatomical localization of implanted subdural electrodes in a virtual reality environment. *J Neurol Surg A Cent Eur Neurosurg*. 2013;74(3):175-82. doi:10.1055/s-0032-1333124.
9. Dalal SS, Edwards E, Kirsch HE, Barbaro NM, Knight RT, Nagarajan SS. Localization of neurosurgically implanted electrodes via photograph-MRI-radiograph coregistration. *J Neurosci Methods*. 2008;174(1):106-15. doi:10.1016/j.jneumeth.2008.06.028.
10. Miyagi Y, Shima F, Sasaki T. Brain shift: an error factor during implantation of deep brain stimulation electrodes. *J Neurosurg*. 2007;107(5):989-97. doi:10.3171/JNS-07/11/0989.
11. King D, Bronen RA, Spencer DD, Spencer SS. Topographic distribution of seizure onset and hippocampal atrophy: relationship between MRI and depth EEG. *Electroencephalogr*

- Clin Neurophysiol.* 1997;103(6):692-7. Available at:  
<http://www.ncbi.nlm.nih.gov/pubmed/9546496>. Accessed January 15, 2014.
12. Pluim JPW, Maintz JBA, Viergever M a. Mutual-information-based registration of medical images: a survey. *IEEE Trans Med Imaging.* 2003;22(8):986-1004. doi:10.1109/TMI.2003.815867.
  13. Hill DL, Batchelor PG, Holden M, Hawkes DJ. Medical image registration. *Phys Med Biol.* 2001;46(3):R1-45. Available at: <http://www.ncbi.nlm.nih.gov/pubmed/11277237>. Accessed August 6, 2013.
  14. R Development Core Team. *R: A language and environment for statistical computing.* Vienna, Austria; 2008. Available at: <http://www.r-project.org>.
  15. Wellmer J, von Oertzen J, Schaller C, et al. Digital photography and 3D MRI-based multimodal imaging for individualized planning of resective neocortical epilepsy surgery. *Epilepsia.* 2002;43(12):1543-50. Available at: <http://www.ncbi.nlm.nih.gov/pubmed/12460257>. Accessed August 12, 2013.
  16. Mahvash M, König R, Wellmer J, Urbach H, Meyer B, Schaller K. Coregistration of digital photography of the human cortex and cranial magnetic resonance imaging for visualization of subdural electrodes in epilepsy surgery. *Neurosurgery.* 2007;61(5 Suppl 2):340-4; discussion 344-5. doi:10.1227/01.neu.0000303992.87987.17.
  17. Tao JX, Hawes-Ebersole S, Baldwin M, Shah S, Erickson RK, Ebersole JS. The accuracy and reliability of 3D CT/MRI co-registration in planning epilepsy surgery. *Clin Neurophysiol.* 2009;120(4):748-53. doi:10.1016/j.clinph.2009.02.002.
  18. LaViolette PS, Rand SD, Ellingson BM, et al. 3D visualization of subdural electrode shift as measured at craniotomy reopening. *Epilepsy Res.* 2011;94(1-2):102-9. doi:10.1016/j.eplepsyres.2011.01.011.
  19. Pieters TA, Conner CR, Tandon N. Recursive grid partitioning on a cortical surface model: an optimized technique for the localization of implanted subdural electrodes. *J Neurosurg.* 2013;118(5):1086-97. doi:10.3171/2013.2.JNS121450.
  20. Dykstra AR, Chan AM, Quinn BT, et al. Individualized localization and cortical surface-based registration of intracranial electrodes. *Neuroimage.* 2012;59(4):3563-70. doi:10.1016/j.neuroimage.2011.11.046.

## FIGURE LEGEND

### **Figure 1: Three-dimensional deformation map of elastic image fusion between an MRI and a CT.**

Green color shows areas of minor deformation whereas red color indicates those with strong deformation. A) Axial section at the level of the temporal lobes. The artifact of subdurally implanted electrode contacts is shown (b). B) Axial section at the level of the frontal lobes. A relevant right frontal pneumocephalus and its effect on the brain tissue are shown (a).

### **Figure 2: Distance between electrode contact center and cortex surface**

The figure shows a highly effective reduction of the distance between the electrode contact centers and the cortical surface, from a median of 2.3 mm to 0 mm after AEF and GEF in the frontal region. Reductions were also measured in the temporal and parietal regions. All reductions are significant (GEF in temporal region:  $p = .03$ ; all others:  $p < .001$ ). Thick lines indicate medians, boxes indicate the interquartile range, and whiskers indicate the  $\pm 1.58x$  interquartile range. Outliers are shown as open circles.

### **Figure 3: Projection of electrode contacts on the brain surface after linear and elastic image fusion**

The figure shows the temporal electrode contacts of two illustrative cases after linear (A and C) and after elastic fusion (B and D). After linear fusion some of the contacts are virtually buried in the tissue. Elastic fusion provides a more plausible projection of the contacts onto the brain surface.

**Table 1: Electrode contacts implanted**

Patient	Laterality	Region	Number of Contacts
1	left	temporo-polar	6
		posterior temporal	6
	right	temporo-polar	6
		anterior temporal	6
		posterior temporal	6
2	left	temporo-polar	4
		anterior temporal	6
		medial temporal	6
		posterior temporal	6
	right	temporo-polar	4
		anterior temporal	6
		medial temporal	6
		posterior temporal	6
3	left	temporo-polar	6
		anterior temporal	6
		medial temporal	6
		posterior temporal	6
	right	temporo-polar	6
		anterior temporal	6
		medial temporal	6
		posterior temporal	6
4	left	temporo-polar	6
		anterior temporal	6
		medial temporal	6
		posterior temporal	6
		inferior frontal	6
		superior frontal	8
		fronto-parietal	8
		parietal	8
	right	temporo-polar	6
		anterior temporal	6
		medial temporal	6
		posterior temporal	6
		inferior frontal	6
		superior frontal	8
		fronto-parietal	8
		parietal	8
5	left	temporo-polar	4
		anterior temporal	6
		medial temporal	6
		posterior temporal	6
	right	temporo-polar	4
		anterior temporal	6
		medial temporal	6
		posterior temporal	6
Total number of contacts implanted			274

Legend: The table shows the positions and numbers of contacts per electrode implanted in each patient.

**Table 2: Midline shift correction**

	No correction	AEF	GEF
Median (mm)	1.90	0	0
IQR	0.75	0.4	0
P		.14 (RF/AEF)	.07 (RF/GEF)
P		.39 (AEF/GEF)	

Legend: The table shows the midline shift measured at the septum pellucidum after AEF and GEF and the results compared with the non-corrected CT.

ACCEPTED

**Table 3: Reduction of frontal pneumocephalus measured as cortex-bone distance**

	No correction	AEF
Median	9.8	9.2
IQR	5.2	4.88
p		.68

Legend: The table shows the maximum thickness of frontal intracranial air measured in an axial slice. The AEF did not lead to a sufficient correction of the brain shift effect.

ACCEPTED



**Table 4: Volumetric reduction of frontal pneumocephalus**

	No correction	Elastic fusion
Median (mm)	19.49	19.1
IQR	20.7	17.18
p		.86

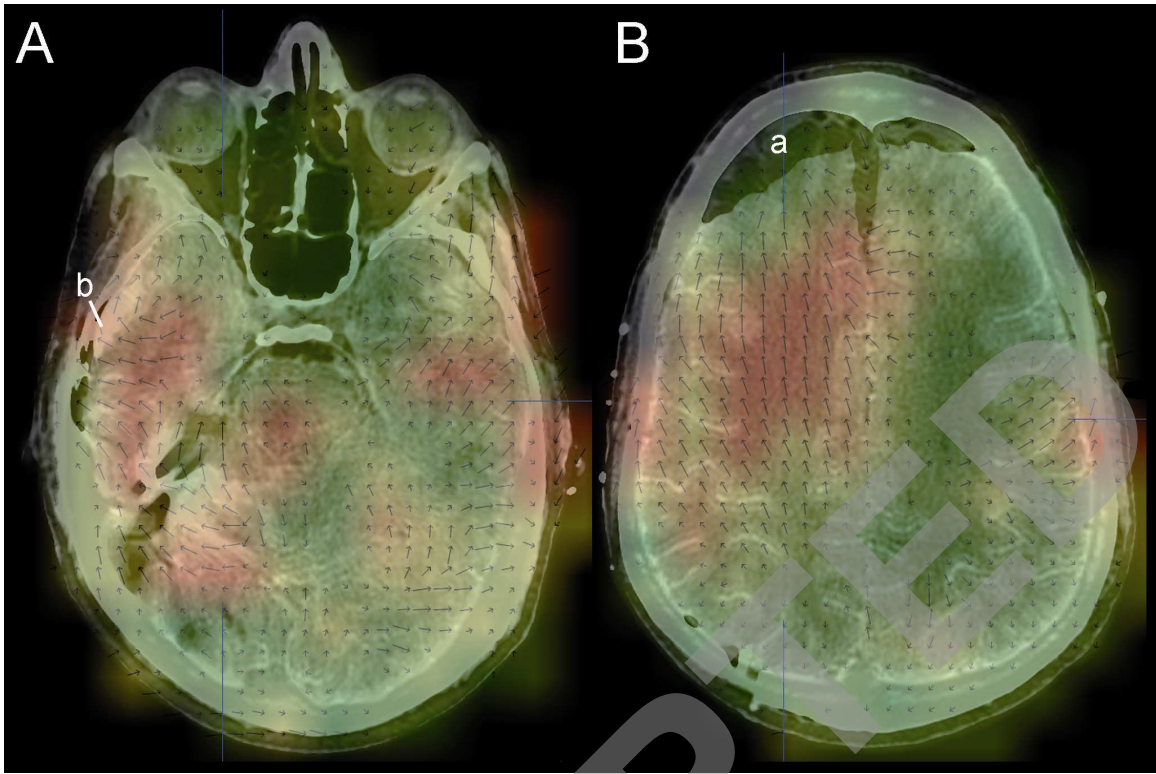
Caption: As a measurement of the pneumocephalus' thickness, the volumetric measurement does not show a satisfying correction of the brain shift effect.

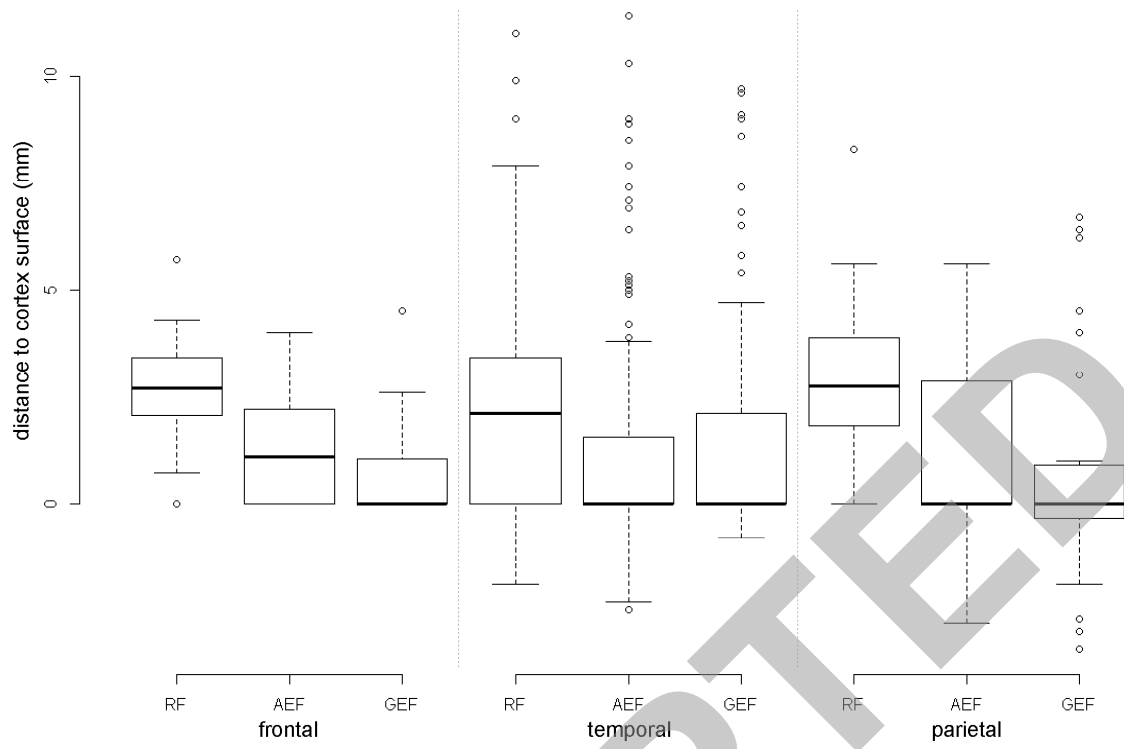
ACCEPTED

**Table 5: Relative correction of electrode contact position by elastic fusion**

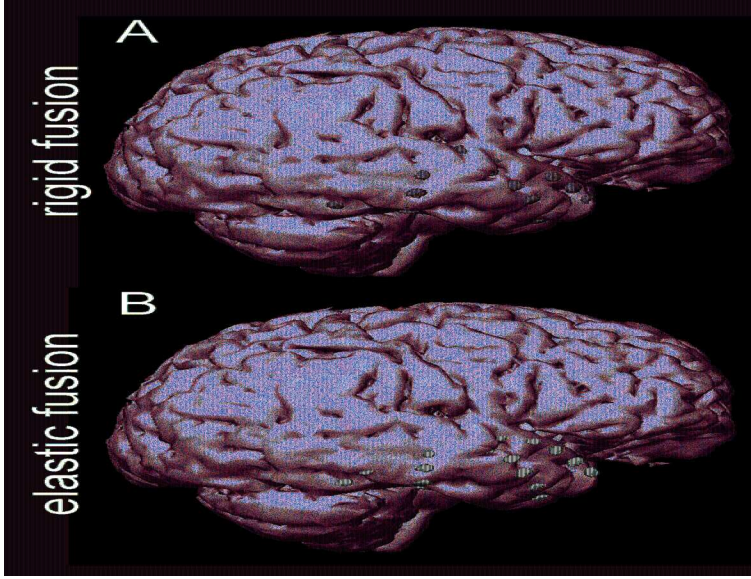
Region:	All		Frontal		Temporal		Parietal	
	AEF	GEF	AEF	GEF	AEF	GEF	AEF	GEF
Median	2.9	2.8	2.45	2.45	2.8	2.6	4.3	4.5
IQR	2.53	2.5	2.1	1.88	2.53	2.45	1.8	2.45
p	.55		.99		.42		.96	
			.031					
					<.001			
			<.001					

Legend: Elastic fusion led to localization of the electrode contacts relative to their original position in the postoperative CT. AEF and GEF achieved nearly identical shifts in all regions. The shift was significantly higher in the temporal than in the frontal region and was greatest in the parietal region.





ACCEPTED



ACCEPTED